García Martínez, A.; Monsalve-Serrano, J.; Lago-Sari, R.; Fogué Robles, Á. (2022). Numerical analysis of kinetic mechanisms for battery thermal runaway prediction in lithium-ion batteries. International Journal of Engine Research. 23(10):1691-1707. https://doi.org/10.1177/14680874211029902

Numerical Analysis of Kinetic Mechanisms for Battery Thermal Runaway Prediction in Lithium-ion Batteries

Antonio García*, Javier Monsalve-Serrano, Rafael Lago Sari and Álvaro Fogué Robles

CMT - Motores Térmicos, Universitat Politècnica de València, Camino de Vera s/n, 46022 Valencia, Spain

International J of Engine Research, 1–17, 2021
DOI: 10.1177/14680874211029902

Corresponding author (*):
Dr. Antonio García Martínez (angarma8@mot.upv.es)
Phone: +34 963876574
Fax: +34 963876574

Abstract

The urgent need for reducing the carbon dioxide emissions has led to the powertrain electrification at different levels such as hybridization or pure electric vehicles. Despite the benefits in terms of local pollution reduction and lower carbon dioxide footprint that may be achieved with this technology, new hazards have been introduced. Among them, the combustion of the battery pack due to abuse conditions, also known as thermal runaway, is one of the biggest concerns. It can lead to the vehicle combustion under unnoticed failure conditions, threating the driver security. In this sense, different investigations have been carried out with the aim of providing a proper description of the reactions that lead to this phenomenon. Reaction mechanisms have been proposed in the literature for lithium-ion battery considering the most common battery chemistries. Nonetheless, their application leads to different results, which may hinder their utilization in modelling critical operating conditions for thermal runaway. This investigation proposes a detailed assessment of the most common reaction mechanisms, comparing their capability on reproducing the different reaction paths that lead to thermal runaway conditions to explore and depict state of the art of thermal runaway modelling. Additionally, a detailed analysis is performed to define the differences in terms of decomposition and formation reactions for each one of them. The results of this investigation demonstrate that the mechanism proposed by Kriston provides the best results trade-off considering different investigations in differential scanning calorimeter and accelerated rate calorimeter. In addition, it was found that some mechanisms have been adjusted to perform similar to the experimental results, even in the case of not having a physical meaning.

Keywords

Battery thermal runaway; vehicle safety; kinetic mechanism; electric vehicles.

1. Background

Different outlooks suggest that the passenger cars energy vectors will change significantly in the next years [1]. While internal combustion engines will be still

dominant [2] and be improved regarding its fuel injection [3][4][5] and combustion system design [6] [7], alternative concepts as plug-in hybrids electric vehicles (PHEV) and battery electric vehicles (BEV) [8]will increase their market share consistently [9] due to their benefits in fuel consumption improvements [10] [11] and emission reductions [12]. This modification is a consequence of the different mandates, that require an effective reduction on the total tank-to-wheel CO_2 emissions [13], which cannot be accomplished by the conventional ICE propelled vehicles[14]. There are associated issues which are referred as market barriers for BEV and PHEV, as the vehicle autonomy and performance at harsh conditions (extreme cold temperatures)[15]. Despite the impact on the technology acceptance, these issues do not imply a hazard to the driver. By contrast, the battery thermal runaway phenomenon concerns to the manufacturers [16], since it may result in a complete vehicle burning in a short time period [17]. This phenomenon can be originated by several type of abuse conditions as mechanical, electrical and thermal abuse [18]. Once an abuse occurs, it gives origin to a chain of reactions that start to decompose the battery compounds in a high exothermic process[19], increasing the temperature of the cell [19]. This process also forms flammable gases and oxygen, which can be ignited by different mechanisms as high local temperatures, short-circuit, etc. [20]. This flame can be sustained out of the cell while the gases are vented and provoke the thermal runaway of the neighbourhood cells [21][22]. Thus, understanding the mechanisms behind the thermal runaway initiation to enable strategies that assure a safe battery operation is of utmost importance[23][24]. In this sense, different authors have provided contributions on the description of this phenomenon, determining the most important reactions in each one of the elements and their impact on the thermal runaway process. To provide a structured discussion, the review of the reactions that take place inside the cell is divided for each one of the elements of the battery.

1.1. Decomposition reactions

As previously introduced, during thermal abuse conditions, the increase of local temperature enables the decomposition of some of the compounds in the battery in an exothermic manner which may enable a chain reaction, i.e., thermal runaway, whenever the temperature levels exceed specific thresholds [25]. The importance of determining the paths that may lead to the thermal runaway have pushed the investigation in this field towards this direction. This led to the specification of dominating routes which are correlated with the main components of the battery cell. They are specified in Figure 1, which is a simplified scheme showing the main parts of a battery cell: cathode, anode, electrolyte and separator. Additionally, the binder also plays a fundamental role on the battery, being responsible for providing a media to intercalate both anode and cathode materials. In the following subsections, the reactions that take place in each one of the parts are described according to different authors.

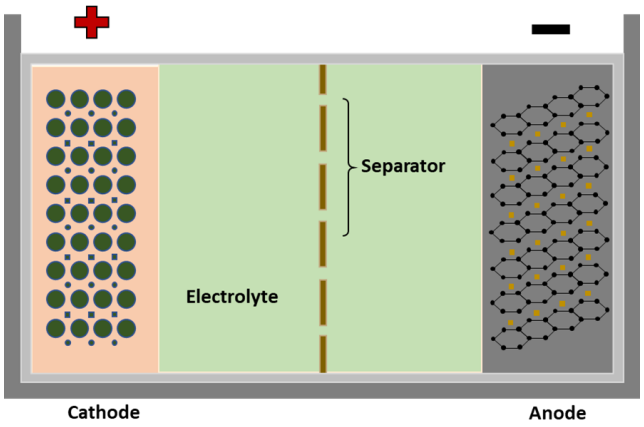

Figure 1. Scheme of a battery cell depicting the cathode, anode and electrolyte.

Solid Electrolyte interface reactions

Solid electrolyte interface (SEI) is originated by the electrochemical reduction of the solvent and electrolyte salt. This reaction is enabled by the contact of the electrolyte with the graphite surface, creating a mixture of several surface species [26]. The resultant layer works as an insulator for the electrons while allowing the flow of Li^+ [27].

Richard and Dahn [28] proposed one of the first mechanisms that describes the different processes that take place in the solid electrolyte interface during a thermal abuse reaction. The SEI is composed by both stable and metastable components. In their investigation, Richard and Dahn have initially considered Li_2CO_3 as stable component and $(CH_2OCO_2Li)_2$ as metastable components, identifying that the last can react as:

$$(CH_2OCO_2Li)_2 \rightarrow Li_2CO_2 + C_2H_4 + CO_2 + \frac{1}{2}O_2 \qquad \text{r.1}$$

or

$$2Li + (CH_2OCO_2Li)_2 \rightarrow 2Li_2CO_3 + C_2H_4 \qquad \text{r.2}$$

The consumption of the metastable component results in heat release, increasing the temperature of the cell. The start of this depletion was verified in temperature values bellow 100 ^oC, with its maximum values around 110 ^oC according to Richard and Dahn [28]. Similar observations were made by different authors as Maleki et al. [29] and Zhang et al. [30]. Yet, Spotnitz and Franklin [31] report that the energy release and the shape of the peak in the process are strongly influenced by the electrolyte composition.

Electrolyte

Reactions accounting for the electrolyte decomposition are not common in reaction mechanisms since there is no clear understating about the role of this component in the temperature increase. Authors as Wang et al. [32] and Campion et al. [33] have found evidence that the electrolyte reacts with LiPF6 salt in temperature ranges from 200 ^oC to 230 ^oC. Nonetheless, these evidences were not observed by Yang et al. [34]. Kriston et al. [35] suggests that his divergence can be a product of the measurement conditions of each experiment. In spite of not being considered in most of the mechanism, several experiments demonstrate a significant energy absorption in the temperature profile evolution near to the temperature ranges of the electrolyte evaporation [36]. Based on

this, Kriston aimed at identifying specific reactions to be included in the mechanism, allowing to capture the effect of the temperature decrease during the electrolyte evaporation.

Graphite anode reactions

Graphite anode has been widely employed as host structure for the lithium-ion in the negative electrode [37]. Nonetheless, as the SEI decomposition occurs, different paths are open for further reactions between the electrolyte, the graphite electrode and the intercalated Li^+. Based on a literature review, Kriston et al. [35] suggested that once the SEI decomposes, ethylene carbonate (EC) may reach the surface of the graphite. Therefore, it can start to react with the intercalated Li^+ by means of different reactions:

$$C_3H_4O_3 + 2Li(C_6) \rightarrow Li_2CO_3 + C_2H_4 \qquad \text{r.3}$$

$$2Li(C_6) + 2EC \rightarrow Li - O - (CH_2)_4 - O - Li + 2CO_2 \qquad \text{r.4}$$

It is interesting to note that both reactions are highly exothermic, resulting in a significant temperature increase. Nonetheless, they originate an inorganic layer that leads to a slowdown of the process. This was evidenced first by Richard and Dahn [28][38], concluding that the reaction with intercalated Li^+ leads to a thicker SEI layer in the electrode surface, as the Li^+ concentration decreases. To account for this phenomenon a two-equation model was proposed by the authors, addressing first a fast-tunneling process that is shifted to a diffusive transport as the SEI thickens. Kriston et al. [35] also suggest that the new SEI prevent further EC-Li reactions for temperatures below 250 ^oC. Nonetheless, as the temperature rises above this threshold, the new SEI is also consumed, contributing to the thermal runaway process. Different from the previous authors, Kriston et al. [35] propose a three-step mechanism to model the anode decomposition.

Cathode reactions

Distinct cathode chemistry such as Nickel-Manganese-Cobalt (NMC) or Li_xCoO_2 are used in battery cells, having different temperature requirements to decompose. Regarding the last chemistry, Biensan et al. [39] reported that the decomposition reactions occur from 220 ^oC to 500 ^oC. A comprehensive investigation has been also performed by Peng [40] and Jiang [41], who have considered 5 different cathode materials ($LiCoO_2$, $LiNi_{0.8}Co_{0.15}Al_{0.05}O_2$, $Li_{1.1}(Ni_{1/3}\text{-}CO_{1/3}\ Mn_{1/3})_{0.9}O_2$, $LiMn_2O_4$), reporting that NMC cathode has one of the highest thermal stability among those evaluated together with the $LiMn_2O_4$, which requires temperatures higher than 275 ^oC to be decomposed.

Li et al. [42] also concluded that the oxygen species suffer irreversible changes during the delithiation process, having great influence on the structural and thermal stability of NMC cathodes. Ren et al. [43] have also monitored the oxygen evolution of the cathode, observing a high oxygen generation from temperatures higher than 200 ^oC. Despite the complex process, in general, the cathode decomposition is approximated by means of a single decomposition reaction. Due to this, Kriston et al. [35] have presented a detailed investigation to understand the decomposition mechanism and propose a multi-step decomposition process of the cathode. From their results, it was inferred that four

different steps are responsible for the cathode decomposition, allowing to propose a multi-step mechanism to capture each one of the important zones. It is also worth to mention that the heat released by the cathode decomposition was significantly lower than that from the anode reactions.

Binder

The binder has a fundamental role in the battery cell, being responsible for gluing the active materials and conductive agent with the current collector [44][45]. Binder is also considered an important compound that decomposes in an exothermic manner, being included in most of the abuse mechanisms for battery cells. Generally, it is accounted inside of the description of both anode and cathode decomposition. Nonetheless, its decomposition is a direct consequence of the temperature increase provided by the reactions that may occur with the anode, cathode and SEI decomposition. In his investigation, Kriston was able to identify the temperature ranges in which the binder that exists in the NMC cathode decomposes, concluding that temperatures in the range from 400 ^{o}C to 500 ^{o}C are required to initiate this reaction. On the anode side, the simultaneous analysis of heat flow and Fourier transformed infrared spectroscopy (FTIR) have allowed kriston et al. to conclude that the binder decomposition occurs at much lower temperatures, from 270 ^{o}C. Different authors have evidenced the reaction of the electrolyte and binder at this temperature range.

From the previous discussion, it can be inferred that the understanding of the chemical reactions that take place inside of the battery cell during abuse conditions is of utmost importance to assure reliable usage of batteries and extend their power density. In spite of that, the available reaction mechanisms still differ in the paths that are considered for the decomposition and consumption of the battery compounds. In this sense, a detailed analysis to understand the differences and impacts of each reaction mechanism must be accomplished.

This investigation aims to propose a numerical tool (TRKIN) to perform detailed assessment of the differences of the most common reaction kinetic mechanisms used for describing the cell abuse and thermal runaway phenomenon for different cell geometries and chemistries. This was accomplished by means of Differential Scanning Calorimeter (DSC) simulations to stress the particularities among different reaction mechanisms regarding the reaction rates of each component under controlled conditions. Both $LiCoO_2$ and NMC cells were investigated with the respective reaction mechanisms. Finally, simulations addressing Accelerate Reaction Calorimeter (ARC) tests were proposed to quantify the impact of the different mechanisms in the prediction of the temperature onset for battery thermal runaway occurrence. To do this, the ARC was operated in oven mode and it was modelled considering the heat transfer balance and reaction kinetics.

2. Tools and methods

This section intends to describe in detail the different battery chemistries that are considered in this investigation as well as the reaction kinetics mechanisms that are used to describe their decomposition. Finally, the solution framework that was developed to accommodate each one of the mechanisms in a single solution environment is described.

2.1. Kinects mechanisms

Different reaction kinetics mechanisms were proposed along the years to describe the concentration evolution of the battery components under abuse conditions. The earlier mechanisms were developed considering cylindrical cell geometries, with $LiCoO_2$ cathode chemistry as the one proposed by Hatchard et al. [46] and later discussed in detail by Kim et al. [47]. Recently, other mechanism has been suggested in the literature for both cylindrical and pouch cell geometries. Among of them, the mechanisms proposed by Ren et al. [36], Feng et al. [48], kriston et al. [35] and Bilyaz [49] have demonstrated to be able to address the thermal runaway process. Despite that, the development process and the reaction modelling differ among them as discussed in the introduction section. The main differences among the different mechanisms are summarized in Table 1. As it can be seen, the mechanism proposed by Kim relies on using 4 reactions in total to describe the thermal runaway process. By contrast, Kriston´s mechanism uses 9 different reactions, providing a more comprehensive relation between the numerical model and the phenomena in discussion.

Table 1. Number of reactions considered in the description of the thermal runaway process for each mechanism used in the investigation.

	Reactions for Anode	Reactions for Cathode	Reactions for Electrolyte	Reactions for Binder	Cat-An interaction
Kim	2	1	1	-	
Kriston	2	2	3	2	
Ren	2	1	-	2	1
Feng	2	2	1	1	1
Bilyatz	2	3	1	2	

2.2. Battery chemistries evaluated

As previously discussed in the introduction section, batteries may be produced considering different compounds in their structure. Generally, lithium-ion batteries use graphite (Gr) as compound for the anode due to its excellent cycling stability [37]. By contrast, a broad spectrum of elements has been reported as possible candidates to be applied for the cathode as $Li[Ni_xCo_yB_{1-x-y}]O_2$ [50] and $LiNi_{0.8}Co_{0.07}Fe_{0.03}Mn_{0.1}O_2$ [51]. Nonetheless, both NMC and $LiCoO_2$ are still two of the most used components for the battery cathode. In this investigation, different chemistries were evaluated according to the reaction mechanism in discussion. Table 2 summarizes the different chemistries for the anode, electrolyte and cathode for each one of the mechanisms that were considered. As it can be seen, both Ren and Feng mechanisms were developed considering the same materials for each cell, being directly comparable. It is also worth to state that, in spite of not specifying EMC in the composition of the electrolyte, it is believed that the mechanism from Kriston can be also compared to the mechanism from Ren et al. and Feng et al.. Themechanism suggested by Kim et al., which relies on the work proposed by Hatchard et al., considers a $LiCoO_2$ composition for the cathode and uses a cylindrical cell with different anode/cathode ratios than the remaining

mechanism, which hinders its comparison with those. Finally, the mechanism proposed by Bilyaz et al. considers the different mechanisms to build its own, without considering the battery chemistry as a prohibitive feature to implement the mechanism. In this sense, this mechanism is herein used only for comparison purposes. As a final remark, it is interesting to remark that the level of detail and component description of each mechanism has been increasing along the years, facilitating the understanding of the mechanism development as well as providing the basis for its comparison and application in real problems.

Table *2*. Compounds of Anode, Cathode, Electrolyte, and binder as well as the geometry of each cell that investigated in this research.

	Anode	**Cathode**	**Electrolyte**	**Binder**	**Geometry**
Kim et al.	Gr	$LiCoO_2$		-	Cylindrical
Kriston et al.	Gr	NMC111	EC:DMC	CMC	-
Ren et al.	Gr	NMC111	EMC:EC:DMC	-	Pouch
Feng et al.	Gr	NMC111	EMC:EC:DMC	-	Pouch
Bilyaz et al.	Gr	$LiCoO_2$	EMC:EC:DMC	CMC*	Pouch*

2.3. TRKIN: Numerical approach

The solution scheme was developed with the aim of providing a global tool in Python®, which may be used to simulate the battery thermal runaway phenomenon by specifying a few input parameters as the battery chemistry, geometry, and mechanism to be used. To do so, the mechanism was implemented in different sub-functions and the Arrhenius coefficients of each reaction (energy of activation and pre-exponential factors) were included as look-up tables for each component and mechanism. Two different devices to assess the mechanisms were developed: a differential scanning calorimeter and an accelerated rate calorimeter, allowing to emulate tests under different conditions. The former was modelled considering a constant heating rate of dT/dt=10 ^{o}C/min. The ARC implementation was made by solving the heat equation for the battery, given by:

$$\frac{dT}{dt} = \frac{1}{m_{bat} \cdot c_p} \cdot \left(m_{active} \cdot \frac{dQ}{dt} + h_{conv} \cdot A \cdot (T_{oven} - T) \right) \qquad \text{Eq.1}$$

The ARC was operated in oven mode, applying different target temperatures to assess the temperature onset at which the thermal runaway begins. Table 3 presents the temperature ranges that were assessed for each mechanism as well as the temperature step, which was defined according to the sensibility of the mechanism according to temperature modifications.

Table 3. Temperature ranges and steps used in oven test evaluation for kriston, Ren and Feng reaction mechanisms.

Mechanism	Temperature Range (ºC)	Temperature Step (ºC)
Kriston et al.	[120-200]	5
Ren et al.	[110-150]	5
Feng et al.	[140-235]	2

Independently on the mechanism, a similar setup was considered regarding the battery and oven thermal properties. Each battery consisted of 1100 g, with a total active material mass of 800 g. The composition of the anode, cathode, electrolyte and binder were given by each mechanism that is evaluated. Finally, the specific heat c_p was set to 1.27 J/g·K, the total heat transfer area A to 0.0841 m^2 and the convective heat transfer coefficient was 7.5 W/m^{2}K for all the tests. Giving the set of boundary conditions to be evaluated, the problem was defined in a differential equation system and solved using the Runge Kutta integrator provided by the Python's library SciPy RK45. Figure 2 presents a schematic representation of the numerical framework that was developed to perform the investigations.

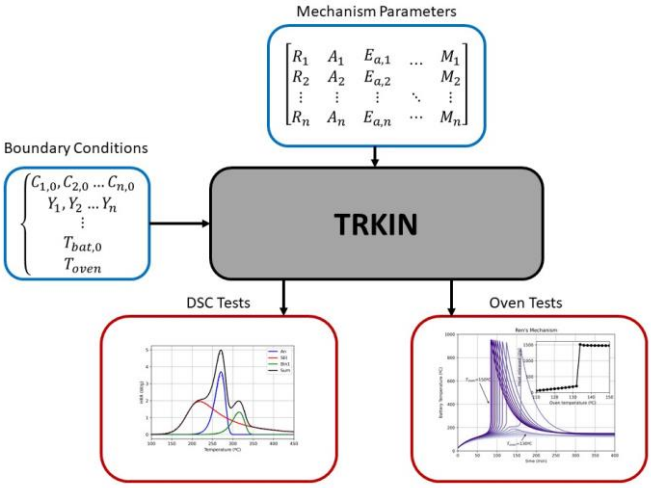

Figure 2. Schematic representation of the solution method and the different devices that were emulated in the TRKIN tool.

2.4. Mechanism implementation

The review of the reaction mechanisms for the thermal runaway description allows to identify different formulations for each one of the decomposition reactions as previously discussed. Nonetheless, the implementation process generally faces different challenges in terms of defining non-reported values by the authors or even small modifications that are not precisely commented. This lack of information can lead to unreasonable results and unsuccessful mechanisms implementation. Therefore, this subsection intends to describe the implementation procedure of each one of the mechanisms. Additionally, a detailed description of the modifications that were done and the different phenomena that needs to be accounted for guaranteeing the reproducibility of the original results is provided. . The final problem formulation for

each mechanism is detailed in Annex A, where the text in bold and Italic stands for the modifications that were done to enable the mechanism implementation.

2.4.1. Kim-Hatchard mechanism

First, the mechanism proposed by Hatchard et al. [46] and reported in a new format by Kim et al. [47] was implemented, considering the set of reactions provided in Annex A. Nonetheless, modifications were made to attain the proper matching that is depicted in Figure 3 due to different issues. Initially, a thermal validation was attempted, consisting of solving the convective heat balance from the oven to the battery cell. Nonetheless, the heating rate that is achieved using the original convective heat transfer as well as the surface area is not able to provide similar results as those from the experiments. Having in mind that the energy balance during the oven test may be described by $Q = h \cdot A \cdot \Delta T$, where h is the convective heat transfer coefficient, A is the cell area for heat transfer and ΔT is the difference between the oven and battery temperature, and the battery heat capacity and mass are known, the heat balance has an analytical solution. Therefore, any difference with respect to the experiments should be a consequence of improper determination of the heat transfer equations. It is worth to mention that the radiation heat transfer is also included by the authors in the original manuscript [47].

To match the thermal behavior at non-reactive conditions a modification in the input parameters of the battery was made. Two different approaches were considered. First, the convective heat transfer coefficient was modified. Nonetheless, the temperature profile differences were not decreased, independently on the value used. Lastly, the surface-to-volume ratio was swept in a broad range of values. The best results were obtained by modifying the surface-to-volume ratio from the original value of 48.37 to 300. With this adjustment, the heating rate of the battery was perfectly matched at the same time of the consumption of the components.

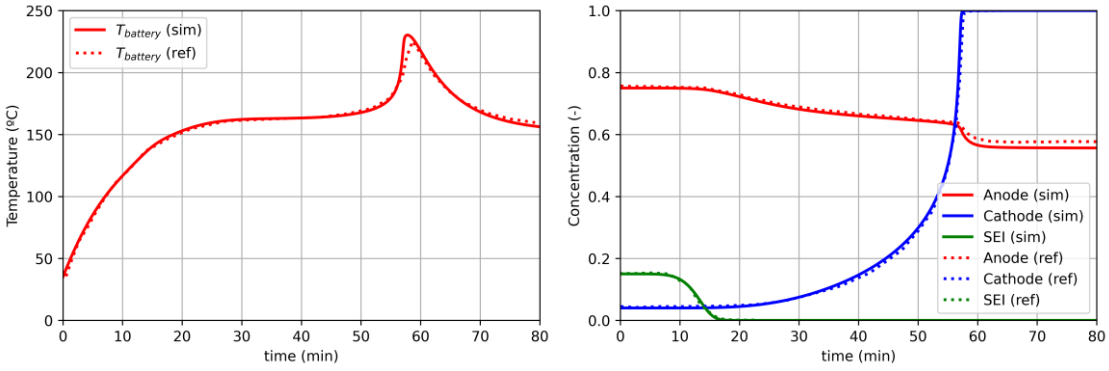

Figure 3. Comparison of simulated and experimental instantaneous temperature evolution (left) and concentration (right) for the Hatchard/Kim mechanism for the oven tests.

2.4.2. Mechanism from Kriston et al.

The mechanism from Kriston et al. [35] has presented the simplest implementation among the mechanisms. This mechanism was developed using DSC tests, having no oven test or ARC evaluation to be compared with. The set of values provided in the manuscript as well as the reactions allowed a proper replication of the heat generation

in the DSC tests, except for the electrolyte vaporization, which was modified to match the first peak of heat release. The results of its implementation compared with those from the experiments are presented in Figure 4. As it can be seen, a good agreement is verified independently on the temperature range evaluated, which is a good indicator of the robustness of the mechanism development.

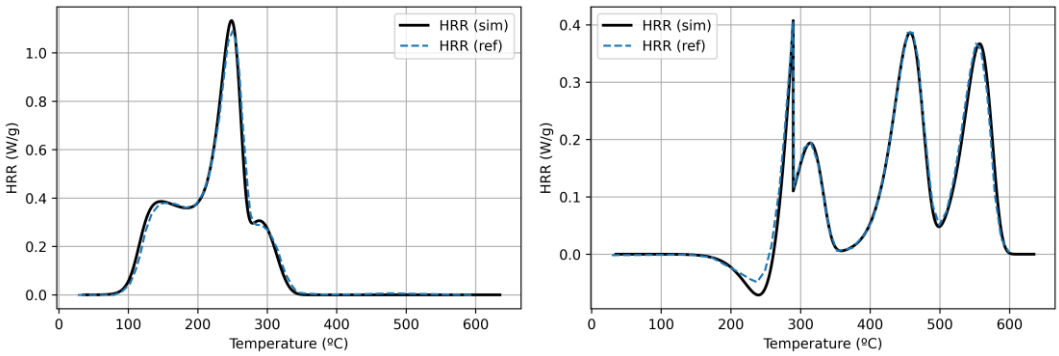

Figure 4. Comparison of simulated and reference (from original manuscript) instantaneous heat release for the anode (left) and cathode+electrolyte (right) components for the mechanism proposed by Kriston et al. in differential scanning calorimeter evaluations.

2.4.3. Mechanism from Ren et al.

The development of the mechanism proposed by Ren et al consisted of both DSC and ARC investigations. Therefore, the implementation was performed in two steps. First, the DSC tests were intended to be replicated with the mechanism provided by the authors (Figure 6). Nonetheless, the authors have used a definition of heating value that is normalized with the total battery mass, which is 9.4 grams. In the case of the anode, the sample was prepared with the same mass as the battery. But for the cathode, the sample mass considered was only 6.8 grams, requiring a rescaling of the energy released by a factor of 1.468 to obtain the same energy output than those of the DSC tests. This small modification has allowed to obtain the same energy release than that presented in the original manuscript.

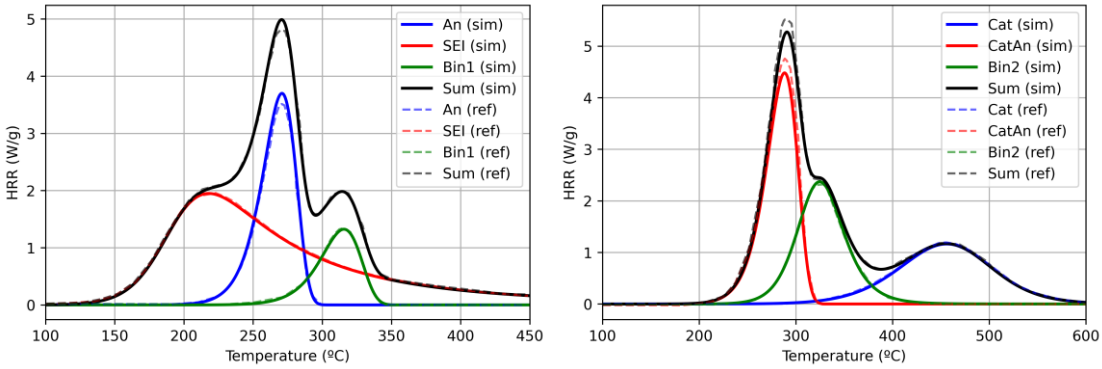

Figure 5. Comparison of simulated and reference (from original manuscript) instantaneous heat release for the anode (left) and cathode (right) reactions for the mechanism suggested by Ren et al. in differential scanning calorimeter evaluations.

The replication of the ARC tests was somewhat difficult (Figure 6). The issues verified can be divided into three different parts. The first problem was related to the lack of

information about the electrolyte evaporation. In spite of mentioning that this phenomenon has a fundamental role in the early stages of the thermal runaway reactions, no specific formulation was proposed. Even though, it is believed that the energy absorption during this phenomenon is considered in the authors calculations. This assumption is based on the fact that the temperature progression and the thermal runaway onset would be not properly matched if the electrolyte evaporation is not considered. Additionally, in the graphs provided by the authors regarding the temperature change rate, a sharp decrease in the heating rate can be observed around 150 ^{0}C, which could be associated to the evaporation of the electrolyte. As a solution for these issues, the inclusion of the electrolyte evaporation equations from the mechanism proposed by Kriston et al. to consider the impact of this component in the problem description is proposed in the current research. The next issue was related to the operating modes of the ARC. Despite presenting an ARC operation in heat-search method, most of the investigations have been performed in oven tests. For these tests, different schemes are presented to define the switching threshold for the different methods (heating, waiting, cooling, etc.). Nonetheless, if the methodology is followed, the oven tests lead to unreasonable results. In this sense, a modification has also done in this work, defining the switch from waiting to cooling mode as always as the battery temperature achieves a value of 20 ^{0}C higher than that of the oven.

Finally, differences were also verified in the cooling phase of the tests if the values reported in the paper are considered to calculate the heat balance. Again, the modelling process of this phenomena is very simple and relies on using a convective heat balance with the oven walls. In this sense, it is believed that the authors are using a much higher cooling rate than that presented in the work. Since the interest of the mechanism is to determine the temperature onset as well as the maximum battery temperature, no correction has been proposed for this issue. In this sense, the temperature evolution during the cooling phase is based on the heat balance inside the oven with the original heat transfer coefficient with a much slower temperature decrease than that presented by the authors in the original manuscript.

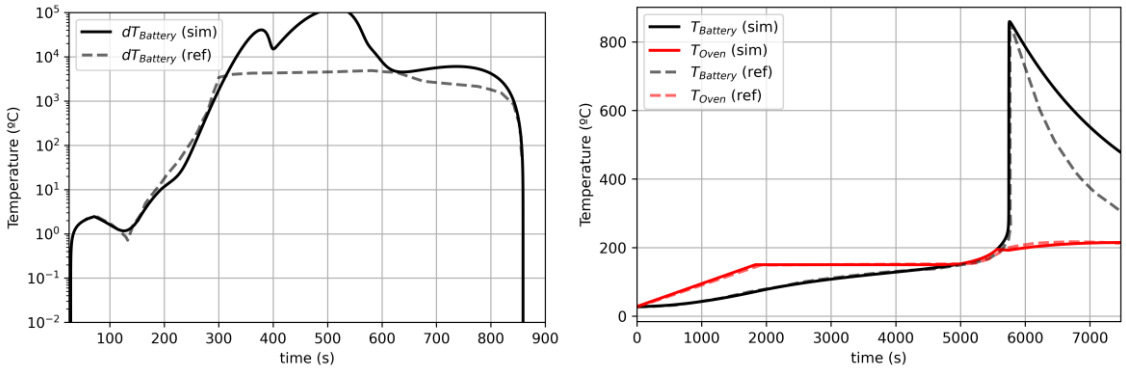

Figure 6. Comparison of simulated and reference (from original manuscript) instantaneous temperature change rate (left) and evolution (right) for the mechanism from Ren et al.

2.4.4. Mechanism from Feng et al.

Feng mechanism validation was not accomplished due to different reasons. The main limiting factor was the absence of important parameters to replicate the accelerate rate calorimeter test that was used in its investigation. In this sense, it was decided to not

pursue the validation of this mechanism. Even though, this mechanism was used for comparison purposes considering the oven tests and DSC investigation proposed by other authors.

2.4.5. Mechanism from Bilyaz et al.

Finally, the mechanism from Bilyaz et al. [49] was implemented considering the set of reactions presented in their work. As commented, the mechanism consists of coupling reactions from the different mechanisms that were previously presented. In this sense, the implementation process is straightforward, obtaining the solid lines presented in Figure 7. As it can be seen, the simulation results match those reported in the original paper most of the time. However, with the information provided in the manuscript, and the set of equations, it is not possible to replicate the discontinuity that is verified in the original work. It is assumed that this type of behavior should come from using specific criteria to limit or even stop certain reactions during the simulation. As this information is not presented in the original work, the present evaluation has considered the original formulation and used this mechanism only for comparison purposes.

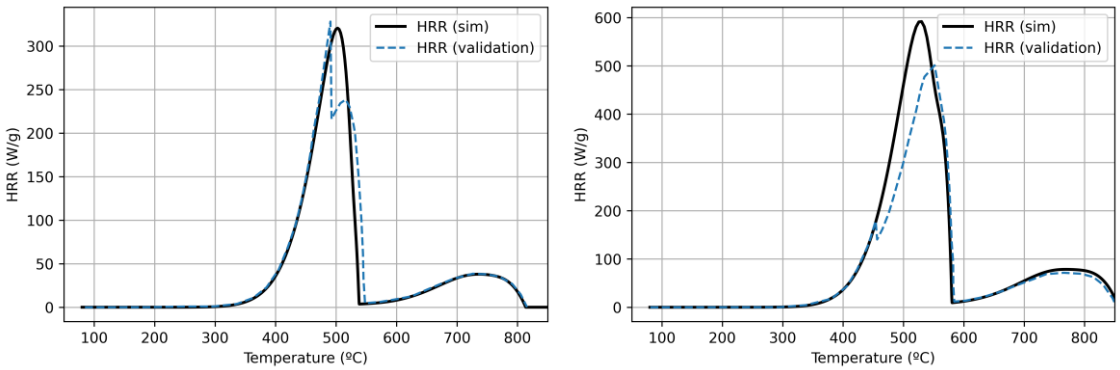

Figure 7. Comparison of simulated and reference (from original manuscript) instantaneous heat release of an oven test at 10 °C/min heating rate (left) and at 100 °C/min heating rate (right) for the mechanism proposed by Bilyaz.

3. DSC analysis of reaction rates

The DSC results for both cathode and anode elements considering the $LiCoO_2$ are presented in Figure 8 for Bilyaz and Kim mechanism. It is worth to mention that the results are presented normalized by the maximum value obtained in each test for each mechanism.

As previously discussed, Bilyaz mechanism is a recompilation of the remaining mechanism, and therefore, its behavior will be the same as the one that was originated from. On the other hand, Kim mechanism considers only four equations to represent the degradation of the components of the cell. Regarding the solid electrolyte interface decomposition, it can be concluded that the start of the reactions occurs at a similar temperature. However, it is evident that the Kim decomposition infers higher energy release in lower temperatures, i.e., the distribution of energy occurs at lower temperature values. This may lead to an early temperature onset during thermal runaway simulation. Since Kim mechanism does not consider further SEI regeneration, the remaining part of the heat that could be observed in the anode is attributed to the

anode decomposition. Nonetheless, as discussed in detail in the introduction section, this does not represent the succession of events that occurs in the SEI. A better description is provided by Kriston, which was therefore, accounted in the Byliaz mechanism. This strategy is argued to be valid since the anode and electrolyte materials are the same in both mechanisms.

In this sense, it is possible to see a second heat release in the Byliaz mechanism that is a consequence of the decomposition of the SEI regenerated in temperature ranges from 120 ºC to 270 ºC which is more relevant than the first SEI degradation. From this temperature a high exothermal process can be observed in the Bilyaz mechanism, comprehending the degradation of the anode and the further reaction of the binder. On the other hand, Kim mechanism has a much earlier peak of heat release which cannot be correlated with any of the reactions observed in Kriston mechanism. Therefore, it is suggested that this mechanism may lead to an early occurrence of thermal runaway.

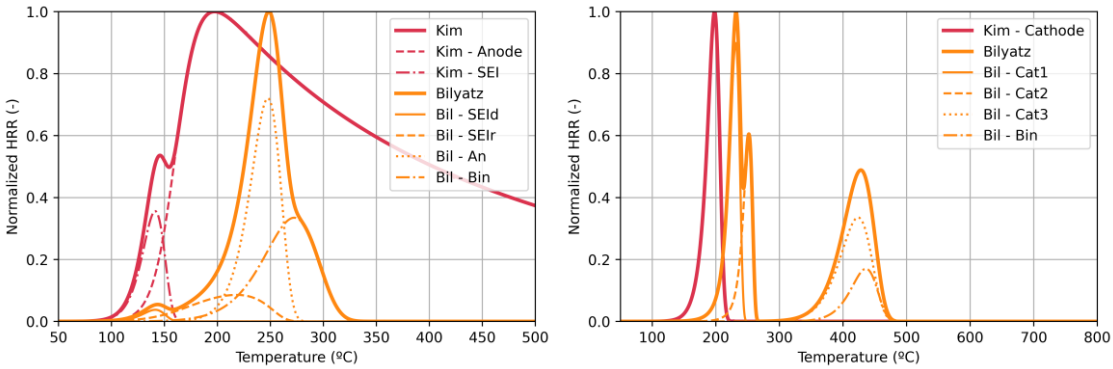

Figure 8 Comparison of instantaneous heat release for the anode and SEI (left hand side) and cathode (right hand side) components for the Bilyaz et al and Kim et al mechanisms in differential scanning calorimeter evaluations.

An early reaction rate is also observed for the cathode reactions. As it is observed in Figure 8 (right), Kim et al. mechanism predicts that the cathode reactions initiate almost 50 ºC earlier than the mechanism proposed by Byliaz et al. Moreover, the single reaction description proposed by Kim et al. also infers a localized heat release in a very narrow temperature range. By contrast, the mechanism from Bilyaz et al. relies on a three-stage decomposition of the cathode. Nonetheless, this approach may be further investigated, since the mechanism considers the equations proposed by kriston et al. to model the cathode decomposition. This mechanism is based on a NMC111 cathode chemistry and some of the phenomenology of the cathode decomposition is a direct consequence of the cell composition, which may hinder the validity of this approach.

The same study was repeated for the NMC 111 cells, applying the mechanisms from Kriston et al., Ren et al. and Feng et al. in DSCs tests. The results of this evaluation are presented in Figure 9. The first interesting observation is the similarity of the mechanisms regarding their peak position and temperature range in which reactions are occurring for the anode material. On the other hand, there is a significant difference in the individual reactions. First, the SEI decomposition starts early for the mechanism proposed by Kriston et al., while the one proposed by ren et al. has a very delayed reaction rate for this component. The mechanism from Ren et al. seems to be in an intermediate temperature range. Nonetheless, its behavior is conditioned by thresholds

which are not necessarily correlated to real phenomena. Both mechanisms proposed by Ren et al. and Kriston et al. present a very similar behavior for the anode decomposition, with clear zones associated with the battery chemistry. The differences among each other can be a direct consequence of the reaction triplet adjustments and the testing method and probes preparation.

Finally, the modelling of the cathode decomposition is compared. As it can be observed in Figure 9 (right), again the mechanisms proposed by Ren et al. and Kriston et al. have a similar distribution of the heat release for the temperature range evaluated. There are some small differences regarding the peak values and the final stage of the heat release curve. The last is a consequence of the addition of a dedicated equation to describe the cathode decomposition and to enhance the modelling of this process by Kriston et al. in their recent work.

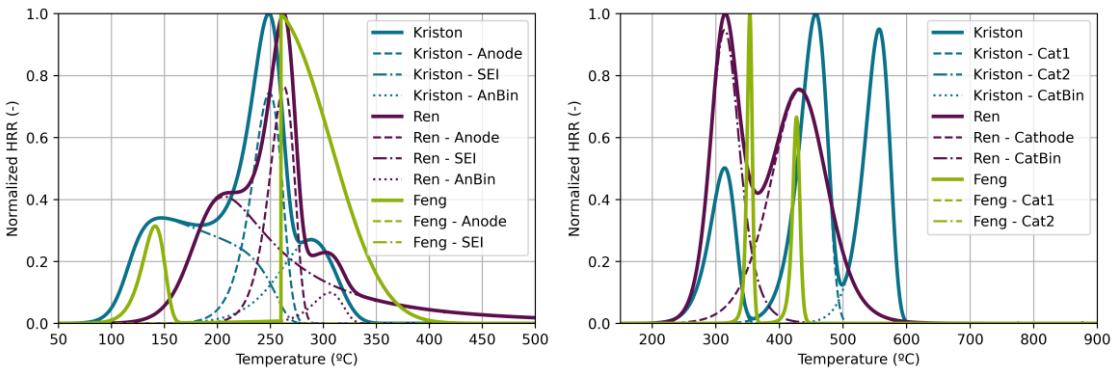

Figure 9. Comparison of instantaneous heat release for the anode and SEI (left) and cathode (right) components for the mechanisms from Kriston et al., Ren et al. and Feng et al. in differential scanning calorimeter evaluations.

From this analysis, it can be observed that the different mechanisms infer distinct heat releases in the conditions that were evaluated. While $LiCoO_2$ battery have very distinct behavior according to the mechanism applied, NMC 111 presents two mechanisms with similar behavior (Kriston et al. and Ren et al.). In this sense, it is believed that the application of them may lead to similar results in the determination of the temperature onset of the thermal runaway phenomenon. It is however interesting to remark that the mechanism from Ren et al. has a more exothermic peak at lower temperatures for the cathode material, which may lead to thermal runaway at lower environment temperatures. To validate this assumption, dedicated analyses in oven test were performed for the different mechanisms and are presented in the next subsection.

4. Mechanisms comparison in oven tests for NMC111 chemistry

As previously discussed, the mechanisms for $LiCoO_2$ chemistry have significant differences in terms of the reaction description and are not able to provide a comparison basis. However, both mechanisms proposed by Ren et al. and Kriston et al., that were developed for the NMC111 cathode chemistry, demonstrated similar results in the DSC tests. Therefore, their performance in quantifying the temperature onset and the thermal runaway description was assessed in oven tests. The mechanism suggested by Feng et al. was also included for comparison purposes since it fulfills the restrictions concerning battery composition. It is worth to mention that the heat transfer

parameters such as convection heat transfer coefficient and environment temperature and ARC characteristics were maintained for all the mechanisms.

Figure 10 presents the results obtained for the oven tests with the mechanism from Kriston et al. To determine the temperature onset, i.e., the temperature at which the battery cell enters in thermal runway, the oven temperature was swept considering values from 120 ^{o}C to 200 ^{o}C in steps of 5 ^{o}C. The analysis of the results allows to identify that at low oven temperatures (≈130 ^{o}C), in spite of having a partial decomposition of the SEI (see Figure 10), the battery does not enter in a thermal runaway process. This can be attributed to the fact that the energy released in the process can be absorbed by the oven. In this sense, as the battery temperature is maintained at low values, the decomposition of the SEI is not fully completed, inhibiting the internal short-circuit associated reactions.

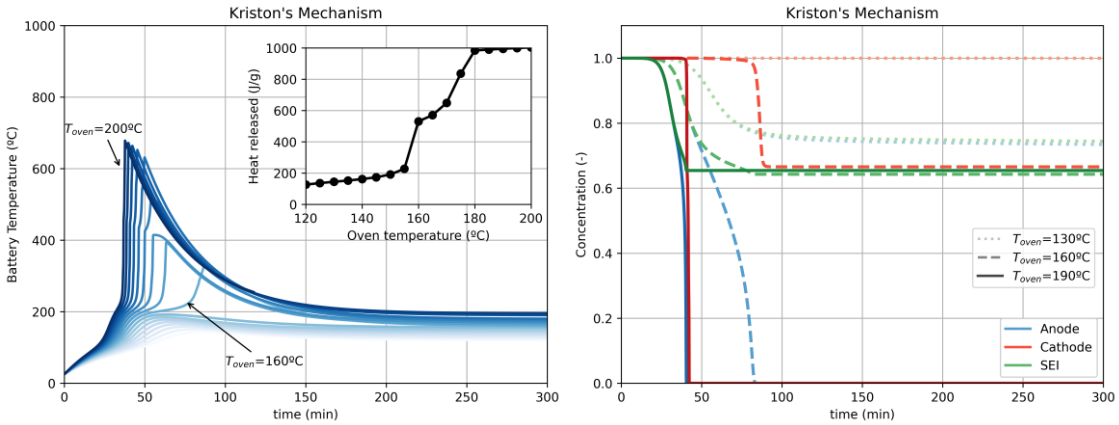

Figure 10. Comparison of simulated and experimental instantaneous temperature evolution (left) and concentration (right) for the Kim et al. mechanism.

Nonetheless, as the temperature is increased, more energy is released by the SEI decomposition promoting a temperature increase and a consequent activation of other reactions such as the anode decomposition. Once the oven achieves the critical temperature value of 160 ^{o}C, the components decomposition leads to a significant temperature increase, achieving the temperature threshold of 200 ^{o}C, which enables the cathode decomposition (the most exothermic process). The abrupt increase of temperature can be observed in the graphs. This is a consequence of the almost exponential increase in the total heat released during the decomposition reactions as shown in Figure 10. In a phenomenological manner, this would be the time where an internal short circuit is enabled, and the anode and the cathode are connected. As it can be observed, the maximum battery temperature achieved once the SEI, cathode and anode are consumed is very similar, with maximum values of almost 700 ^{o}C.

The next mechanism evaluated is the one proposed by Ren et al. The first remarkable difference is the required temperature values to enable the thermal runaway. While the mechanism from Kriston et al. only reaches this condition with oven temperatures of 160 ^{o}C, the mechanism from Ren et al. already fulfill conditions for BTR at 136 ^{o}C. This can be justified by both the results from the DSC evaluation (Figure 9) and those presented in Figure 11. The former has allowed to conclude that the mechanism suggested by Ren et al. predicts a delayed decomposition of the anode with respect to the results provided by the mechanism proposed by Kriston et al. Nonetheless, as

previously discussed, the energy released by the anode decomposition is a small fraction compared to that originated in the cathode reaction. This last reaction has a much earlier peak for the mechanism proposed by Ren et al., which may be one of the reasons for a lower temperature onset compared to the mechanism suggested by Kriston et al. It is also worth to mention that the mechanism from Ren et al. also predicts a higher SEI decomposition for the case of 130 ^{o}C. This may seem contradictory with the previous results provided in the DSC evaluation. Nonetheless, it is important to remark that the DSC results are shown in a normalized basis, which may hinder the visualization of low heat releases of the SEI. Additionally, the SEI decomposition predicted by Ren lasts for a longer temperature range. If a fixed time of observation, e.g., 150 min, is considered, each mechanism provides similar results in terms of SEI concentration. Once the oven temperature is slightly increased (6 ^{o}C), the battery enters in thermal runaway because of the early cathode decomposition. The heat release analysis for each oven temperature allows to identify an almost binary behavior, much more abrupt than the one obtained with the mechanism suggested by Kriton et al. This may lead to stiffness problems, since low time steps are required in the solution to capture this transition.

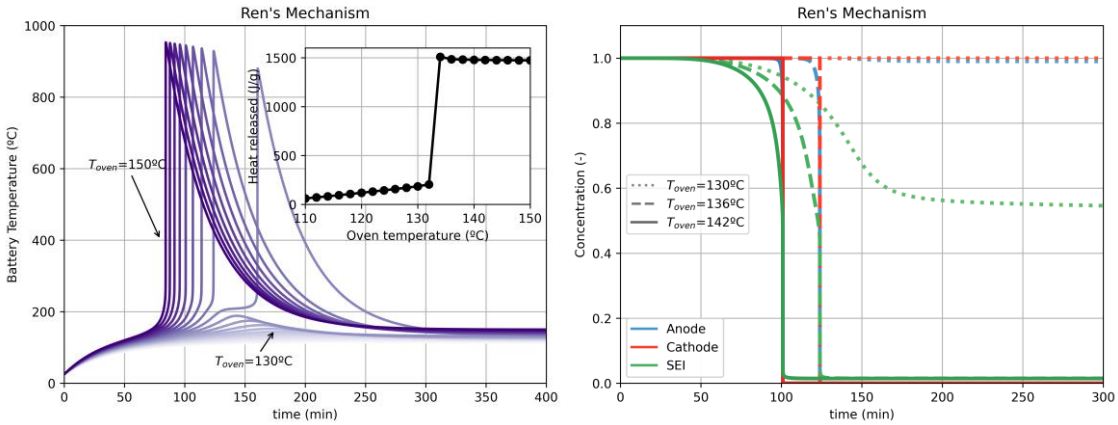

Figure 11 Comparison of simulated and experimental instantaneous temperature evolution (left) and concentration (right) for the Ren et al. mechanism.

Finally, the mechanism proposed by Feng et al. was assessed considering the proposed oven test configuration. As it can be observed in Figure 12, this mechanism presents the highest temperature onset for thermal runaway prediction, requiring oven temperatures higher than 200 ^{o}C to observe the phenomena. The analysis of both concentration graphs of Figure 12 (right) and the heat released for each oven temperature allows to conclude that there is a wide range of temperatures where the mechanism has a constant reaction rate. This is justified by the fact that the mechanism considers a temperature threshold to activate the cathode decomposition reaction. In this sense, despite of the temperature increases from 175 ^{o}C to 210 ^{o}C, no noticeable difference is perceived in the battery temperature. This feature leads to a non-physical relation between the issue and the modelling approach.

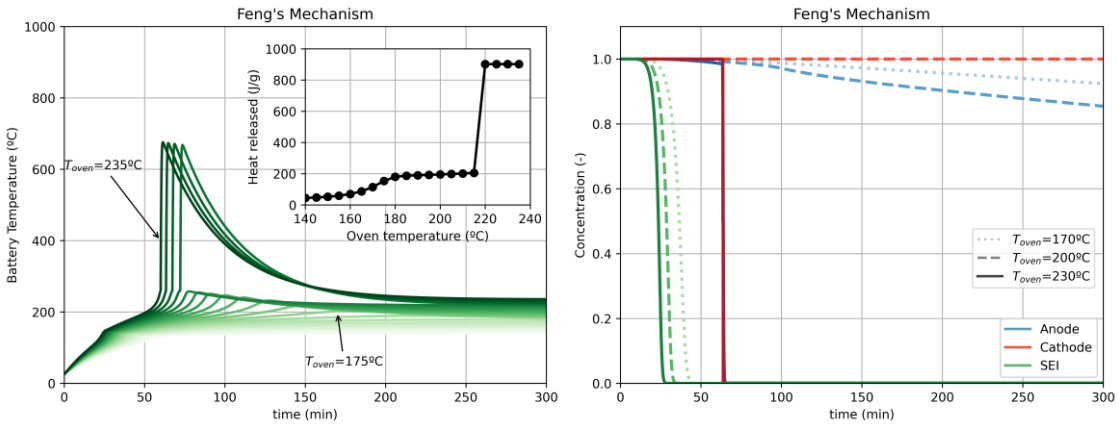

Figure 12. Comparison of simulated and experimental instantaneous temperature evolution (left) and concentration (right) for the Feng et al. mechanism.

Considering the results of the analysis provided by the three mechanisms, it can be argued that remarkable differences are obtained for both temperature onset and concentration evolution. From a conservative perspective, the mechanism suggested by Ren et al. seems to be more suitable, since it results in low temperature onsets. Nonetheless, this may be a consequence of oversimplification of the reaction paths. Kriston et al. mechanism, with a more detailed mechanism, presents a less binary behavior compared with that from Ren et al. and Feng et al., avoiding discontinuities in the solution. The temperature onset presented by Kriston et al. mechanism is higher than that from Ren et al., but still aligned with the results from fundamental investigations in DSCs. Each mechanism presents a good accuracy on reproducing their own experiments. However, as introduced in the methodology section, several tuning parameters were identified, mainly for the mechanism suggested by Ren et al. In this sense, further experimental investigations are required to avoid biased comparisons and asses the accuracy of each reaction mechanism in describing the experimental temperature evolution. It is also interesting to remark that this modelling approach can also be coupled with advanced and robust control strategies as the one proposed by Wang et al. [52] enhancing the vehicle safety. Table x summarizes the advantages and disadvantages of each mechanism based on the considerations evidenced in both DSC and ARC evaluations.

	Advantages	**Disadvantages**
Kim-Hatchard	-Widely studied and validated, including CFD simulations.	-Simple to be extended to other batteries. - Dependent on heat transfer definition. -No effect from binder and cathode-anode interaction.
Kriston	-At the moment is the most complex one. -Includes different phenomena related to evaporation and oxidation that can affect thermal runaway. -Consistent with a good explanation of the most relevant stages during thermal runaway.	-Only defined for DSC tests. -No validation on oven tests with the complete battery. -No reaction associated to cathode-anode reactions.
Ren	-Includes several reactions related to binder degradation and anode-cathode reaction -Reaction's definition is consistent with the physics.	-No reactions related to electrolyte. -Needs definition of electrolyte evaporation.

		-Oven tests have been a challenge due to discrepancies in the definition of the test procedure.
Feng	-Includes several reactions related to binder degradation and anode-cathode reaction.	-Unnatural behavior of the reactions due to defining a piecewise function for the parameters. -SEI reactions have significantly lower impact on BTR prediction compared to other mechanisms. -Cathode reactions do not follow the same trends that can be found in the literature.
Bilyatz	-Includes a variety of reactions.	-Inconsistent in the selection of mechanisms as they do not match the experimental composition -Inconsistent in the selection of reactions as they are defined and validated for different battery compositions within the same battery element.

5. Conclusions

This manuscript has presented a detailed investigation addressing the effect of reaction mechanism in the prediction of battery thermal runaway phenomena using an in-house built Python plug-in (TRKIN). A comparison considering differential scanning calorimeter and accelerated rate calorimeter simulations was performed for each mechanism considering batteries with different cathode chemistry to obtain an evaluation of the status of thermal runaway modelling. The DSC investigations have allowed to draw important conclusions about the decomposition reactions::

- The comparison of mechanisms for $LiCoO_2$ has shown that the modeling approach for the thermal runaway can differ significantly in terms of anode and cathode decomposition.
- The modelling of battery thermal runaway for NMC111 chemistry cathode shows much lower dispersion in the temperature range for decomposition. Nonetheless, the peak of the reactions differs in some extent, which may lead to differences in the temperature onset description.
- The mechanism proposed by Kriston et al. provides the most phenomenological description of the processes which occur in the different components, including reactions for phenomena that are generally not considered in the remaining mechanism as the case of electrolyte decomposition.

Finally, the ARC investigations have allowed to understand the impact of having different reaction rates for similar battery chemistry regarding the occurrence of battery thermal runaway phenomena for NMC 111 chemistry. The main findings can be summarized as:

- It was demonstrated that despite of small differences in the DSC, the results from ARC presents significant differences in the thermal runaway prediction.

- Both mechanisms proposed by Ren et al. and Feng et al. have provided an almost binary behavior between conditions that have TR and conditions where TR is not present.
- The mechanism suggested by Kriston et al. seems to have more continuity between the reactions. This highlights the importance of selecting a robust mechanism for assess the early reactions that may indicate the thermal runaway, assuring the safety and providing the required time to employ protective measures.

In this sense, it can be concluded that this papers has successfully implemented and compared the most relevant thermal runaway mechanisms for $LiCoO_2$ and NMC cathode chemistries. The differences evidenced in this work highlights the need of dedicated investigations to improve the accuracy and agreement of the mechanism. To do this, further investigations are still required to compare the results from simulation with those from experiments to avoid a biased comparison with the original papers.

References

[1] ExxonMobil. 2019 Outlook for energy: a perspective to 2040. 2019.

[2] Reitz RD, Ogawa H, Payri R, Fansler T, Kokjohn S, Moriyoshi Y, et al. IJER editorial: The future of the internal combustion engine. Int J Engine Res 2020;21:3–10. https://doi.org/10.1177/1468087419877990.

[3] Payri R, De La Morena J, Monsalve-Serrano J, Pesce FC, Vassallo A. Impact of counter-bore nozzle on the combustion process and exhaust emissions for light-duty diesel engine application. Int J Engine Res 2019;20:46–57. https://doi.org/10.1177/1468087418819250.

[4] Payri R, Gimeno J, Martí-Aldaraví P, Viera A. Measurements of the mass allocation for multiple injection strategies using the rate of injection and momentum flux signals. Int J Engine Res 2021;22:1180–95. https://doi.org/10.1177/1468087419894854.

[5] Bermúdez V, García A, Villalta D, Soto L. Assessment on the consequences of injection strategies on combustion process and particle size distributions in Euro VI medium-duty diesel engine. Int J Engine Res 2020;21:683–97. https://doi.org/10.1177/1468087419865652.

[6] Molina S, García A, Monsalve-Serrano J, Villalta D. Effects of fuel injection parameters on premixed charge compression ignition combustion and emission characteristics in a medium-duty compression ignition diesel engine. Int J Engine Res 2021;22:443–55. https://doi.org/10.1177/1468087419867014.

[7] Krishnasamy A, Gupta SK, Reitz RD. Prospective fuels for diesel low temperature combustion engine applications: A critical review. Int J Engine Res 2020. https://doi.org/10.1177/1468087420960857.

[8] Hooper PR. Low noise, vibration and harshness solutions for in-line three-cylinder range extender and hybrid electric vehicles. Int J Engine Res 2021;22:581–91. https://doi.org/10.1177/1468087419859084.

[9] International Energy Agency (IEA). Global EV Outlook 2020: Entering the decade of electric drive? Glob EV Outlook 2020 2020:273.

[10] Luján JM, García A, Monsalve-Serrano J, Martínez-Boggio S. Effectiveness of hybrid powertrains to reduce the fuel consumption and NOx emissions of a Euro 6d-temp diesel engine under real-life driving conditions. Energy Convers Manag 2019;199:111987. https://doi.org/10.1016/j.enconman.2019.111987.

[11] Benajes J, García A, Monsalve-Serrano J, Martínez-Boggio S. Optimization of the parallel and mild hybrid vehicle platforms operating under conventional and advanced combustion modes. Energy Convers Manag 2019;190:73–90. https://doi.org/10.1016/j.enconman.2019.04.010.

[12] García A, Monsalve-Serrano J, Martinez-Boggio S, Gaillard P, Poussin O, Amer AA. Dual fuel combustion and hybrid electric powertrains as potential solution to achieve 2025 emissions targets in medium duty trucks sector. Energy Convers Manag 2020;224:113320. https://doi.org/10.1016/j.enconman.2020.113320.

[13] Telles S, Reddy SK, Nagendra HR. A European Strategy for Low-Emission Mobility. Eur Com 2019;53:1689–99.

[14] Kalghatgi GT. The outlook for fuels for internal combustion engines. Int J Engine Res 2014;15:383–98. https://doi.org/10.1177/1468087414526189.

[15] Smith D, Graves R, Ozpineci B, Jones PT, Lustbader J, Kelly K, et al. Medium-and Heavy-Duty Vehicle Electrification: An Assessment of Technology and Knowledge Gaps 2019:85.

[16] Liu T, Liu Y, Wang X, Kong X, Li G. Cooling control of thermally-induced thermal runaway in 18,650 lithium ion battery with water mist. Energy Convers Manag 2019;199:111969. https://doi.org/10.1016/j.enconman.2019.111969.

[17] Liu H, Wei Z, He W, Zhao J. Thermal issues about Li-ion batteries and recent progress in battery thermal management systems: A review. Energy Convers Manag 2017;150:304–30. https://doi.org/10.1016/j.enconman.2017.08.016.

[18] Feng X, Zheng S, Ren D, He X, Wang L, Liu X, et al. Key characteristics for thermal runaway of Li-ion batteries. Energy Procedia 2019;158:4684–9. https://doi.org/10.1016/j.egypro.2019.01.736.

[19] Golubkov AW, Planteu R, Krohn P, Rasch B, Brunnsteiner B, Thaler A, et al. Thermal runaway of large automotive Li-ion batteries. RSC Adv 2018;8:40172–86. https://doi.org/10.1039/C8RA06458J.

[20] Ostanek JK, Li W, Mukherjee PP, Crompton KR, Hacker C. Simulating onset and evolution of thermal runaway in Li-ion cells using a coupled thermal and venting model. Appl Energy 2020;268:114972. https://doi.org/10.1016/j.apenergy.2020.114972.

[21] Li W, Wang H, Ouyang M, Xu C, Lu L, Feng X. Theoretical and experimental analysis of the lithium-ion battery thermal runaway process based on the internal combustion engine combustion theory. Energy Convers Manag 2019;185:211–22. https://doi.org/10.1016/j.enconman.2019.02.008.

[22] Yang X, Duan Y, Feng X, Chen T, Xu C, Rui X, et al. An Experimental Study on Preventing Thermal Runaway Propagation in Lithium-Ion Battery Module Using Aerogel and Liquid Cooling Plate Together. Fire Technol 2020;56:2579–602. https://doi.org/10.1007/s10694-020-00995-x.

[23] Weng J, Ouyang D, Yang X, Chen M, Zhang G, Wang J. Alleviation of thermal runaway propagation in thermal management modules using aerogel felt coupled with flame-retarded phase change material. Energy Convers Manag 2019;200:112071. https://doi.org/10.1016/j.enconman.2019.112071.

[24] Sun Q, Wang Q, Zhao X, Sun J, Lin Z. Numerical study on lithium titanate battery thermal response under adiabatic condition. Energy Convers Manag 2015;92:184–93. https://doi.org/10.1016/j.enconman.2014.12.019.

[25] Li Q, Yang C, Santhanagopalan S, Smith K, Lamb J, Steele LA, et al. Numerical investigation of thermal runaway mitigation through a passive thermal management system. J Power Sources 2019;429:80–8. https://doi.org/10.1016/j.jpowsour.2019.04.091.

[26] Guo Y. Encyclopedia of Electrochemical Power Sources. Encycl Electrochem Power Sources 2009:241–53.

[27] Agubra VA, Fergus JW. The formation and stability of the solid electrolyte interface on the graphite anode. J Power Sources 2014;268:153–62. https://doi.org/10.1016/j.jpowsour.2014.06.024.

[28] Richard MN, Dahn JR. Accelerating Rate Calorimetry Study on the Thermal Stability of Lithium Intercalated Graphite in Electrolyte. II. Modeling the Results and Predicting Differential Scanning Calorimeter Curves. J Electrochem Soc 1999;146:2078–84. https://doi.org/10.1149/1.1391894.

[29] Maleki H, Deng G, Anani A, Howard J. Thermal Stability Studies of Li-Ion Cells and Components. J Electrochem Soc 1999;146:3224–9. https://doi.org/10.1149/1.1392458.

[30] Zhang Z, Fouchard D, Rea JR. Differential scanning calorimetry material studies: Implications for the safety of lithium-ion cells. J Power Sources 1998;70:16–20. https://doi.org/10.1016/S0378-7753(97)02611-6.

[31] Spotnitz R, Franklin J. Abuse behavior of high-power, lithium-ion cells. J Power Sources 2003;113:81–100. https://doi.org/10.1016/S0378-7753(02)00488-3.

[32] Wang QS, Sun JH, Chu GQ, Yao XL, Chen CH. Effect of LiPF6 on the thermal behaviors of four organic solvents for lithium ion batteries. J Therm Anal Calorim 2007;89:245–50. https://doi.org/10.1007/s10973-006-7534-1.

[33] Campion CL, Li W, Lucht BL. Thermal Decomposition of LiPF[sub 6]-Based Electrolytes for Lithium-Ion Batteries. J Electrochem Soc 2005;152:A2327. https://doi.org/10.1149/1.2083267.

[34] Yang H, Zhuang G V., Ross PN. Thermal stability of LiPF6 salt and Li-ion battery electrolytes containing LiPF6. J Power Sources 2006;161:573–9. https://doi.org/10.1016/j.jpowsour.2006.03.058.

[35] Kriston A, Adanouj I, Ruiz V, Pfrang A. Quantification and simulation of thermal decomposition reactions of Li-ion battery materials by simultaneous thermal analysis coupled with gas analysis. J Power Sources 2019;435:1–13. https://doi.org/10.1016/j.jpowsour.2019.226774.

[36] Ren D, Liu X, Feng X, Lu L, Ouyang M, Li J, et al. Model-based thermal runaway prediction of lithium-ion batteries from kinetics analysis of cell components. Appl Energy 2018;228:633–44. https://doi.org/10.1016/j.apenergy.2018.06.126.

[37] Asenbauer J, Eisenmann T, Kuenzel M, Kazzazi A, Chen Z, Bresser D. The success story of graphite as a lithium-ion anode material-fundamentals, remaining challenges, and recent developments including silicon (oxide) composites. Sustain Energy Fuels 2020;4:5387–416. https://doi.org/10.1039/d0se00175a.

[38] Richard MN, Dahn JR. Accelerating rate calorimetry studies of the effect of binder type on the thermal stability of a lithiated mesocarbon microbead material in electrolyte. J Power Sources 1999;83:71–4. https://doi.org/10.1016/S0378-7753(99)00260-8.

[39] Biensan P, Simon B, Pérès JP, De Guibert A, Broussely M, Bodet JM, et al. On safety of lithium-ion cells. J Power Sources 1999;81–82:906–12. https://doi.org/10.1016/S0378-7753(99)00135-4.

[40] Peng P, Jiang F. Thermal safety of lithium-ion batteries with various cathode materials: A numerical study. Int J Heat Mass Transf 2016;103:1008–16. https://doi.org/10.1016/j.ijheatmasstransfer.2016.07.088.

[41] Jiang J, Dahn JR. ARC studies of the thermal stability of three different cathode materials: LiCoO2; Li[Ni0.1Co0.8Mn0.1]O 2; and LiFePO4, in LiPF6 and LiBoB EC/DEC electrolytes. Electrochem Commun 2004;6:39–43. https://doi.org/10.1016/j.elecom.2003.10.011.

[42] Li J, Zhang ZR, Guo XJ, Yang Y. The studies on structural and thermal properties of delithiated LixNi1/3Co1/3Mn1/3O2 ($0 < x \leq 1$) as a cathode material in lithium ion batteries. Solid State Ionics 2006;177:1509–16. https://doi.org/10.1016/j.ssi.2006.03.055.

[43] Ren D, Liu X, Feng X, Lu L, Ouyang M, Li J, et al. Model-based thermal runaway prediction of lithium-ion batteries from kinetics analysis of cell components. Appl Energy 2018;228:633–44. https://doi.org/10.1016/j.apenergy.2018.06.126.

[44] Shi Y, Zhou X, Yu G. Material and Structural Design of Novel Binder Systems for High-Energy, High-Power Lithium-Ion Batteries. Acc Chem Res 2017;50:2642–52. https://doi.org/10.1021/acs.accounts.7b00402.

[45] Chou SL, Pan Y, Wang JZ, Liu HK, Dou SX. Small things make a big difference: Binder effects on the performance of Li and Na batteries. Phys Chem Chem Phys 2014;16:20347–59. https://doi.org/10.1039/c4cp02475c.

[46] Hatchard TD, MacNeil DD, Basu A, Dahn JR. Thermal Model of Cylindrical and Prismatic Lithium-Ion Cells. J Electrochem Soc 2001;148:A755. https://doi.org/10.1149/1.1377592.

[47] Kim GH, Pesaran A, Spotnitz R. A three-dimensional thermal abuse model for lithium-ion cells. J Power Sources 2007;170:476–89. https://doi.org/10.1016/j.jpowsour.2007.04.018.

[48] Feng X, He X, Ouyang M, Lu L, Wu P, Kulp C, et al. Thermal runaway propagation model for designing a safer battery pack with 25Ah LiNixCoyMnzO2 large format lithium ion battery. Appl Energy 2015;154:74–91. https://doi.org/10.1016/j.apenergy.2015.04.118.

[49] Bilyaz S, Marr KC, Ezekoye OA. Modeling of Thermal Runaway Propagation in a Pouch Cell Stack. Fire Technol 2020;56:2441–66. https://doi.org/10.1007/s10694-020-00970-6.

[50] Ryu HH, Park NY, Yoon DR, Kim UH, Yoon CS, Sun YK. New Class of Ni-Rich Cathode Materials Li[NixCoyB1−x−y]O2 for Next Lithium Batteries. Adv Energy Mater 2020;10:1–8. https://doi.org/10.1002/aenm.202000495.

[51] Zha G, Hu W, Agarwal S, Ouyang C, Hu N, Hou H. High performance layered LiNi0.8Co0.07Fe0.03Mn0.1O2 cathode materials for Li-ion battery. Chem Eng J 2021;409:128343. https://doi.org/10.1016/j.cej.2020.128343.

[52] Wang S, Fernandez C, Yu C, Fan Y, Cao W, Stroe DI. A novel charged state prediction method of the lithium ion battery packs based on the composite equivalent modeling and improved splice Kalman filtering algorithm. J Power Sources 2020;471:228450. https://doi.org/10.1016/j.jpowsour.2020.228450.

Abbreviations and symbols

A	Area
BEV	Battery Electric Vehicles
BTR	Battery Thermal Runaway
C2H4	Ethylene
CO2	Carbon Dioxide
DMC	Dimethyl Carbonate
DSC	differential scanning calorimeter
EC	ethylene carbonate (EC),
EMC	ethyl methyl carbonate
FTIR	Fourier transformed infrared spectroscopy
Gr	graphite
hconv	Convective heat transfer coeffiecients
ICE	Internal Combustion Engine
Li	Lithium
NMC	Nickel-Manganese-Cobalt
O	Mononuclear Oxygen
O2	Oxygen
PHEV	plug-in hybrids electric vehicles
Q	Heat

SEI	Solid electrolyte interface
T	Temperature
TR	Thermal Runaway

APPENDIX

Kim et al. mechanism

The general formulation to determine the reaction rates is given by r.5. It is used independently n the mechanism. Each parameter can be replaced in the equation according to the tables that follows. It is worth to mention that the parameters modified with respect to the original mechanism are marked by a bold and italic font.

$$R_x = A_x \cdot (c_x)^{n_1} \cdot (1 - c_x)^{n_2} \cdot e^{\frac{E_{a,x}}{R^0 \cdot T}} \cdot g_x \qquad \text{r.5}$$

Where,

$$R^0 = 8.3145 \frac{J}{K \cdot mol}$$

Table 4 Parameters for the mechanism proposed by Kim.

Reaction	x	$C_{x,0}$	A_x	$E_{a,x}$	n_1	n_2	Δh_x	g_x	$Y_{x,0}$	T_{onset}
		[-]	[1/s]	[kJ/mol]	-	-	[J/g]			°C
SEI decomp	SEI	0.15	$1.667 \cdot 10^{15}$	135.08	1	0	257	1	0.273	-
An+Ele	An	0.75	$2.5 \cdot 10^{13}$	135.08	1	0	1714	$e^{-t_{sei}/t_{sei,0}}$	0.273	-
Cat decomp	Cat	0.04	$6.667 \cdot 10^{13}$	139.6	1	1	***251.2***	1	0.546	-
Ele decomp	E	1	$5.14 \cdot 10^{25}$	274	1	0	155	1	0.182	-

Table 5 Initial concentrations of the components considered in the Kim mechanism.

	dc/dt	C0
Anode	-Ran	0.75
Cathode	-Rcat	0.04
Electrlyte	-Re	1
SEI	-Rsei	0.15
t_{SEI}	-Ran	0.033
Binder	-	

Table 6 Thermal parameters that were considered in the Kim mechanism.

Battery Test Parameters	
AVratio	***300***
H	7.17
Epsilon	0.8
Sigma	$5.6703744 \cdot 10^{-8}$
Rho·cp (J/m^3 K)	$2.789 \cdot 10^{6}$
Toven,0 (ºC)	***152.2***
Tbat,0 (ºC)	35

Kriston et al. mechanism

Table 7 Parameters for the mechanism proposed by Kriston.

Reaction	x	$C_{x,0}$	A_x	$E_{a,x}$	n_1	n_2	Δh_x	g_x	$Y_{x,0}$	T_{onset}
		[-]	[1/s]	[kJ/mol]	-	-	[J/g]			°C
SEI decomp	An	1	$1.67 \cdot 10^{15}$	1348.96	1	0	1312	$e^{-t_{sei}/t_{sei,0}}$	0.46	-
An+Ele	An	1	$1.78 \cdot 10^{14}$	1619.96	1	0	479.397	1	0.46	-
An+Bin decomp	Bin	1	$5.62 \cdot 10^{6}$	963.55	1	0	208.15	1	0.46	-
Cat1 decomp	Cat1	1	$3.22 \cdot 10^{10}$	1415.21	1	0	100.02	1	1	-
Cat+Bin decomp	Cat2	1	$3.78 \cdot 10^{12}$	2053.56	1	0	212.9	1	1	-
Cat3 decomp	Cat3	1	$1.3 \cdot 10^{6}$	2890.64	1	0	189.02	1	1	-
Ele evap	Ele	1	$2.23 \cdot 10^{7}$	951.50	1	0	***-62.5***	1	1	-
Ele decomp	Ele	1	$5.14 \cdot 10^{25}$	22763.79	1	0	155	1	1	-
Ele oxidation	Ele, O2	1	$5.14 \cdot 10^{18}$	1264.66	1	0	2000	$[c_{O_2}]^{n_1}$	1	-

Table 8 Initial concentrations of the components considered in the Kriston mechanism in the cathode.

	dc/dt	C0
Anode	-Ran-Rsei	1
Cathode	(-Rcat1-Rcat2-Rcat3)/3	1
Electrlyte	-Re,ev-Re,ox-Re,dec	1
SEI	-Rsei	1
t_{SEI}	Rsei	0.033
Binder	-Ran,b	1

Table 9 Initial concentrations of the components considered in the Kriston mechanism in the anode.

	dc/dt	C0
Cat1	-Rcat1	1
Cat2	-Rcat2	1
Cat3	-Rcat3	1
O2	Rcat2*Ko2-Rele,ox	0

$$K_{O_2} = \frac{22}{75} \cdot \frac{32}{82} = 0.114472$$

Ren et al. mechanism

Table 10 Parameters for the mechanism proposed by Ren.

Reaction	x	$C_{x,0}$	A_x	$E_{a,x}$	n_1	n_2	Δh_x	g_x	$Y_{x,0}$	T_{onset}
		[-]	[1/s]	[kJ/mol]	-	-	[J/g]			°C
SEI decomp	Sei	1	$6.3623 \cdot 10^9$	109.6	5.5	0	578.7	1	1	-
An+Ele	An	1	$5.151 \cdot 10^{17}$	200.77	1	0	253.2	1	1	-
An+Bin decomp	BinAn	1	$4.9679 \cdot 10^{15}$	195.49	1	0	108.5	1	1	-
Cat decomp	Cat	1	$5.3481 \cdot 10^5$	109.34	1.5	0	434	1	1	-
Cat+Bin decomp	BinCat	1	$6.5429 \cdot 10^{13}$	177.85	2	0	452.1	1	1	-
Cat+An	An	1	$2.4262 \cdot 10^{13}$	162.01	1	0	560.6	1	1	-
Ele evap	***Ele***	***1***	***$2.23 \cdot 10^7$***	***951.50***	***1***	***0***	***-150***	***1***	***1***	***-***

Table 11 Initial concentrations of the components considered in the Ren mechanism in the cathode and anode.

	dc/dt	C0
Anode	-Ran-Rcatan	1
Cathode	-Rcat	1
Electrlyte	-Re,ev	1
SEI	-Rsei	1
t_{SEI}	-	-
Binder	-(g/(g+1))*RbinAn-(1/(g+1))RbinCat	1

Table 12 Initial concentrations of the components considered in the Ren mechanism in the binder.

	dc/dt	C0
BinAn	-RbinAn	1
BinCat	-RbinCat	1

Feng et al. mechanism

Table 13 Parameters for the mechanism proposed by Feng.

Reaction	x	$C_{x,0}$	A_x	$E_{a,x}$	n_1	n_2	Δh_x	g_x	$Y_{x,0}$	T_{onset}
		[-]	[1/s]	[kJ/mol]	-	-	[kJ/g]			°C
SEI decomp	Sei	1	$1.667 \cdot 10^{15}$	135.08	1	0	257	1	0.147	50
SEI regen	An	1	1	0	0	0	0	5*Ran	0.147	50
An+Ele decomp	An	1	T<260; 0.038 T>260;5	33	1	0	1714	$e^{-c_{sei}/t_{sei,0}}$	0.147	50
Separator melt	Bin	1	$1.5 \cdot 10^{50}$	420	1	0	-190	1	0.0257	120
Cat1 decomp	Cat1	0.999	$1.75 \cdot 10^9$	141.95	1	1	77	1	0.2614	180
Cat2 decomp	Cat2	0.999	$1.077 \cdot 10^{12}$	158.88	1	1	84	1	0.2614	220
Ele decomp	Ele	1	$1.5 \cdot 10^{13}$	150	1	0	800	1	0.1577	120
AnCat react	x	x	1	0	0	0	0.1·(30800/685-Hcatan)	1	0.6698	260

Table 14 Initial concentrations of the components considered in the Feng mechanism in the cathode and anode.

	dc/dt	C0
Anode	-Ran	1
Cathode	(-Rcat1-Rcat2)/2	1
Electrlyte	-Rele	1
SEI	-Rseid+Rseir	1
t_{SEI}	-	0.15
Binder	-Rbin	1

Table 15 Initial concentrations of the components considered in the Feng mechanism in the cathode.

	dc/dt	C0
Cat1	-Rcat1	0.999
Cat2	-Rcat2	0.999

Bilyatz et al. mechanism

Table 16 Parameters for the mechanism proposed by Byliaz.

Reaction	x	$C_{x,0}$	A_x	$E_{a,x}$	n_1	n_2	Δh_x	g_x	$Y_{x,0}$	T_{onset}
		[-]	[1/s]	[kJ/mol]	-	-	[kJ/g]			°C
SEI decomp	Sei	0.1	$1.667 \cdot 10^{15}$	135.1	1	0	613	1	0.0375	-?
SEI regen	An	0.75	$1.667 \cdot 10^{6}$	77.2	1	0	1330	$\left(\frac{t_{sei,0}}{t_{sei}}\right) \cdot e^{-t_{sei}/t_{sei,0}}$	0.0542	-?
An+Ele decomp	An	0.75	$1.78 \cdot 10^{14}$	161.7	1	0	479.397	1	0.238	-?
BinAn decomp	BinAn	1	$5.62 \cdot 10^{6}$	93.5	1	0	208.15	1	0.238	-?
Cat1 decomp	Cat1	0	$1.27 \cdot 10^{10}$	113.8	0	1	470	$\mathrm{Ln}(1 - c_{cat1})^{2/3}$	0.44	-?
Cat2 decomp	Cat2	0	$2.33 \cdot 10^{12}$	140.7	0	1	280	$\mathrm{Ln}(1 - c_{cat2})^{2/3}$	0.44	-?
Cat3 decomp	Cat3	0	$5.71 \cdot 10^{9}$	159.3	0	1	500	1	0.44	-?
BinCat decomp	BinCat	1	$3.78 \cdot 10^{12}$	199.5	1	0	212	1	0.44	-?

Table 17 Initial concentrations of the components considered in the Byliaz mechanism in the cathode and anode.

	dc/dt	C0
Anode	-Ran-Rseir	0.75
Cathode	(-Rcat1-Rcat2-Rcat3)/3	0.94
Electrlyte	-	-
SEI	-Rseid	0.1
t_{SEI}	Rseir	0.15
Binder	(-RbinAn-RbinCat)/2	1

Table 18 Initial concentrations of the components considered in the Byliaz mechanism in the cathode and binder.

	dc/dt	C0
Cat1	Rcat1	0.03
Cat2	Rcat2	0.03
Cat3	Rcat3	0
BinAn	-RbinAn	1
BinCat	-RbinCat	1